

No Calibration, No Depth, No Problem: Cross-Sensor View Synthesis with 3D Consistency

Cho-Ying Wu, Zixun Huang, Xinyu Huang, Liu Ren

Bosch Research North America & Bosch Center for Artificial Intelligence (BCAI)

{Cho-Ying.Wu, Zixun.Huang, Xinyu.Huang, Liu.Ren}@us.bosch.edu

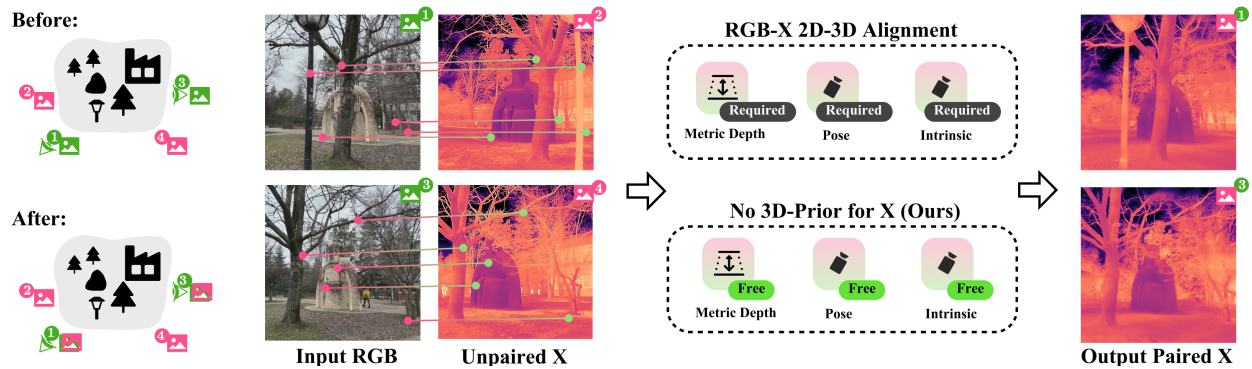


Figure 1. **Problem Setup.** Given unpaired RGB-X images from sensors, the task is to synthesize X-images that are pixel-wise aligned with the RGB views for multi-modal applications. Traditional 3D approaches rely on complete 3D priors—including depth and the poses/intrinsics of both modalities—to align and render cross-sensor images. In contrast, our scalable framework removes these dependencies, enabling RGB-guided X-image synthesis without the 3D priors for X to replace calibration for different types of sensors and metric depth acquisition.

Abstract

We present the first study of cross-sensor view synthesis across different modalities. We examine a practical, fundamental, yet widely overlooked problem: getting aligned RGB-X data, where most RGB-X prior work assumes such pairs exist and focuses on modality fusion, but it empirically requires huge engineering effort in calibration. We propose a match-densify-consolidate method. First, we perform RGB-X image matching followed by guided point densification. Using the proposed confidence-aware densification and self-matching filtering, we attain better view synthesis and later consolidate them in 3D Gaussian Splatting (3DGS). Our method uses no 3D priors for X-sensor and only assumes nearly no-cost COLMAP for RGB. We aim to remove the cumbersome calibration for various RGB-X sensors and advance the popularity of cross-sensor learning by a scalable solution that breaks through the bottleneck in large-scale real-world RGB-X data collection. See [project page](#).

1. Introduction

Sensors other than the RGB spectrum are useful for various applications, such as NIR (Near-Infrared) sensors for night

vision in autonomous driving [9, 12, 47, 57], or thermal sensors for leak detection or robust autonomous systems [22, 30, 39, 43, 56, 58]. Although with diverse applications, they remain relatively underexplored in research. First, they are much less in data quantity compared with RGB, and the research on other sensors needs to rely on their paired and view-aligned RGB to provide rich information from foundation models for scene understanding [19, 62, 102]. For sensors such as thermal cameras, images are natively low-texture and rely on RGB to provide features.

However, real data captured by different sensors typically suffer from multiple issues, making it challenging to build an RGB-X paired dataset, where X denotes other types of sensors in the work. The traditional industrial settings leverage 3D reprojection, which requires **cumbersome sensor calibration** including *measuring intrinsics*, *sensor synchronization*, *relative pose estimation*, and *metric depth*, where errors within each stage will be propagated and affect the end results, and it still cannot solve occlusion from displacement.

Structure-from-motion methods like COLMAP [70] are widely used in scene reconstruction and considered much less effort in sensor calibration. Yet, it only works on RGB scenes and usually fails to work on X or RGB-X settings, particularly on less-texture sensors such as thermal cameras.

The RGB-X systems usually require additional high-

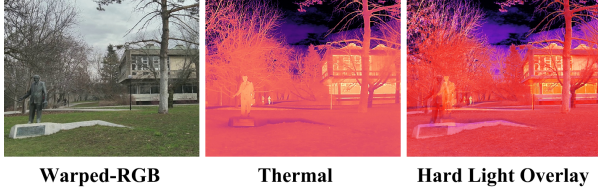


Figure 2. Homography warping assumes 3D planar structures and causes visible misalignment (statue areas) when the scene contains distinct fore-/background layers.

precision dense depth sensors, such as RGB-Thermal-Depth system [41], but it further complicates sensor registration efforts and is not scalable. Some datasets simply consider fixed depth [54] for re-projection without solving the rooted issue. Note that RGB-D systems already encode 3D information that can be re-projected to RGB’s view (still requiring intrinsics and limited by depth sensor precision and density), while other sensors without such 3D priors cannot.

Some recent work performs cross-modality matching of keypoints between RGB and X views [66, 79, 95] based on RGB image matchers. However, they either produce sparse or incomplete correspondences or have highly noisy matches in low-confidence regions. Their goal is to estimate the camera pose or homography matrix $H \in \mathcal{R}^{3 \times 3}$ for warping, where a target view pixel p' and source view pixel p (both in homogeneous coordinates) are related by $p' = H^{-1}p$. However, homography warping assumes *3D planar structures*, indicating it can only distort or shear the view as a plane but cannot create 3D effects with disparity. The warping works when the scene lies around a depth layer, but will show distinct misalignment in counterexamples (See Fig. 2).

This work is **the first scalable framework for cross-sensor view synthesis** to acquire paired and aligned RGB-X data without cumbersome calibration or metric depth, to facilitate the research on sensors **without 3D priors and beyond RGB cameras** (Fig. 1), such as *Thermal Cameras*, *NIR Cameras*, and *Synthetic-Aperture Radar (SAR)*.

First, we adopt cross-modal image matchers to match keypoints between RGB and X views and accumulate X’s keypoints across frames onto the current RGB view to form an aligned sparse or semi-dense X-map. Then, both the RGB and X-map are input to our trained RGB-guided X-densifier, which reconstructs the dense X-map. With a handful of keypoints aggregated in X-map and RGB images as guidance, the model generates a dense X-image that satisfies the input X-map and infills the void areas using RGB and surrounding points as cues. However, we find that densification may lead to irregular or noisy structures affected by noisy matches in low-confidence areas. A higher confidence threshold yields a sparser X-map that must rely more on cross-domain guidance from RGB, while a lower threshold introduces noisy X-points and distorts structures. We propose **Confidence-Aware Densification and Fusion (CADF)** that densifies and

fuses multi-level threshold X-maps into one X-image.

Then, we perform patch rejection by our **self-matching** mechanism—We look into the patch features from the image matcher with the prior that each patch should be matched to the same patch for RGB-X pairs. We calculate a similarity matrix between each patch and reject low-similarity patches. After that, we perform a finer-stage densification. To further enhance multi-view consistency, we adopt RGB-X 3D Gaussian Splatting (3DGS) on RGB’s views to consolidate in the 3D space for multi-view consistency. The work only considers running COLMAP on RGB for 3DGS training, which is standard and considered no-cost. In the experiments, we further show that even without using 3DGS, we still attain better performance than others.

Contributions. Our contributions are as follows.

- The first scalable framework for cross-sensor view synthesis on RGB-X to get view-aligned pairs without calibration or depth—studying a fundamental but widely overlooked problem in prior cross-modal/sensor learning.
- A *match-densify-consolidate* framework. It begins with matched sparse keypoints and presents a densification approach with our CADF module that integrates matching confidence into the densifier for better synthesis, followed by subsequent filtering, re-densification, and 3DGS to build up 3D consistency.
- Extensive evaluation demonstrating our method attains the state of the art on the methods without 3D priors, even still outperforming them without leveraging 3DGS.

2. Related Work

2.1. RGB-X Task and Data Curation

Imaging sensors beyond RGB like NIR or thermal cameras are useful in industrial applications, especially in autonomous driving for adverse weather or night vision to ensure safety [7, 31, 40, 61, 71, 73]. Some works study sensor fusion strategy for segmentation, detection, or tracking [13, 14, 23, 26, 27, 29, 34, 42, 52, 53, 75, 76, 81, 87, 93, 97, 99, 100, 104, 105] and applications in robotics [2, 20, 33, 49, 55, 98]

Most works focus on sensor fusion and design fusion modules. However, they all assume **pixel-wise aligned RGB-X inputs already**, which require substantial engineering effort in sensor calibration, synchronization, and precise metric depth from sensors like Lidar or ToF to help alignment. Some works adopt image translation from RGB to generate X-images, such as RGB-to-thermal, to get pseudo-paired data [1, 6, 45, 92]. They do not use real information in X, and the generation needs to deal with inherent ambiguity. E.g., a cup of water can be flexible in its exact temperature (cool or cold) and hard to judge by its appearance.

In contrast to prior works, we focus on this fundamental problem in data and propose a scalable framework to reduce

the engineering effort to obtain paired RGB-X real data.

2.2. Cross-Modal Image Matching

Image matching is a fundamental problem. Early methods adopt handcrafted descriptors [8, 77] and find a transformation with RANSAC [21]. During the deep learning era some works adopt CNN [16, 17, 60, 80, 82], graph neural network [69, 72, 101], transformers [11, 59, 74, 84], lightweight attention [51, 64], or benefit from foundation models [18, 32]. They focus on matching in the RGB domain from different views, and performance severely degrades for cross-modal matching. Further, image matching aims for relative pose estimation and still needs 3D priors such as intrinsics and precise metric depth for re-projection. Without 3D priors, they still use an estimated homography matrix to warp to the target view, which is confined by its underlying assumption (Fig. 2).

Recent feed-forward reconstruction methods, like DUST3R [85], VGGT [83], or MapAnything [37], also implicitly predicts intrinsics, depth, and 3D pointmap and reconstructs the scene. However, they cannot perform cross-modal matching, and reconstruction would fail due to feature dissimilarity.

Few works have explored cross-modal matching. ReD-Feat [15] uses an adapter and detector to get features and compute detection scores for RGB-thermal pairs. XoFTR [79] uses transformers for coarse-to-fine RGB-thermal matching and achieves stronger performance. MIN-IMA [66] presents a cross-modal image generation engine (e.g., RGB-to-thermal) to finetune image matchers, such as LightGLUE [51] as its featured model, thereby enhancing feature robustness across modalities. However, they still estimate poses or homography matrices and remain confined by the assumptions behind.

3. Methods

We enable RGB-X cross-sensor view synthesis without requiring 3D priors for X, such as scene metric depth and calibration for cross-sensor relative pose and intrinsics (Fig. 1).

Detailed method is shown in Fig. 3. We begin with the smallest components— pixel-level keypoints from a cross-modal image matcher— and perform RGB-X densification to generate X-images aligned with RGB. Our Confidence-Aware Densification and Fusion (CADF) module integrates image-matching confidence into the densification stage to achieve better synthesis. Then, we propose self-matching for filtering, where we use the matcher as an evaluator to filter out erroneous patches, followed by finer-stage re-densification. Lastly, we employ RGB-X 3DGS using RGB camera poses along with densified and aligned X-view, and consolidate both sensors into an unified 3D space. Notably, the pipeline only requires cheap and widely-used COLMAP

on RGB. We show that even without 3DGS and COLMAP, our densified maps still outperform baselines in experiments.

3.1. RGB-X Matching

Matching. Given an RGB image \mathcal{I} and X-modality image \mathcal{X} , image matching finds a matching set that maps coordinates $p^{\mathcal{I}}$ in \mathcal{I} to $p^{\mathcal{X}}$ in \mathcal{X} with a confidence score c . Most matchers can afford sparse or semi-dense matching in practice, where memory consumption directly scales with the number of candidates. The matching results are filtered by a threshold δ , where a match is kept when $c >= \delta$.

Cross-modal matchers typically yield far fewer correspondences than RGB-based ones. This is partly due to the inherent challenge of aligning features across modalities. Further, modalities like thermal or SAR often contain large homogeneous regions (e.g., uniform-temperature areas lacking surface texture), making it difficult to extract feature points for reliable matching.

We begin from an image matcher and stack N frames’ X-keypoints into corresponding RGB’s coordinates to get \mathcal{X}_m .

$$\mathcal{X}_m[p] = \frac{\sum_n \mathbf{1}[p = p_n^{\mathcal{I}}] \mathcal{X}[p_n^{\mathcal{X}}]}{\sum_n \mathbf{1}[p = p_n^{\mathcal{I}}]}, \quad (1)$$

where $n \in N$, and $\mathbf{1}[\cdot]$ is the indicator function that equals 1 if the condition holds and 0 otherwise. If $p \neq p_n^{\mathcal{I}}, \forall n \in N$, $\mathcal{X}_m[p] = -1$, meaning void area.

Area Sampling. To ameliorate matching in texture-less or complex areas, such as sky, ground, walls, or grass, we adopt GroundedSAM [67] to segment these areas on RGB images. Then, we uniformly sample points from the corresponding warped X-images (via homography) within the mask and still void areas. To prevent warping errors from heavily influencing subsequent densification, and to allow erroneous matches to be filtered out later, we only sample 5% points of such areas.

$$\mathcal{X}_m[p] = \mathcal{X}_W[p], \quad p \sim U(\{p \mid \mathcal{M}(p) = 1 \wedge \mathcal{X}_m[p] = -1\}), \quad (2)$$

where U is uniform sampling, \mathcal{X}_W denotes the warped X-image to RGB view, using a homography matrix computed from RGB-X correspondences, and \mathcal{M} is the area mask.

3.2. Confidence-Aware Densification and Fusion

Densification. The obtained \mathcal{X}_m is sparse/ semi-dense, and then we densify it by a network D to get a dense map. D is pretrained on diverse RGB-X modalities using paired data, where the model takes an RGB image along with a down-sampled, sparsified X-map as inputs. The model is trained to densify X into a dense map. The architecture contains a backbone of recurrent units [106, 107] and dynamic spatial propagation (DySPN) layers [50] that refine the output with spatial attention from known points in a recurrent fashion. For inference, \mathcal{I} and \mathcal{X}_m are inputs. Using a handful of points as cues in \mathcal{X}_m , D generates a better dense map

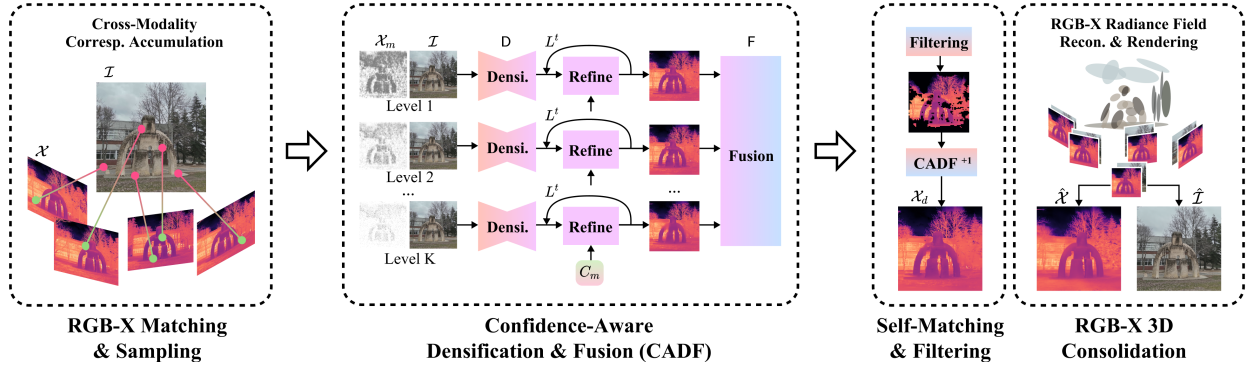


Figure 3. **Method Overview.** Our approach consists of three stages. In the first stage, we perform *cross-modality feature matching* to establish correspondences between RGB and X-images. The matched points are sampled and accumulated onto RGB views to produce semi-dense X-images \mathcal{X}_m along with multi-level confidence maps C_m . In the second stage, we conduct RGB-guided densification to get dense X-images from RGB with semi-dense X as cues. Our Confidence-Aware Densification and Fusion module integrates confidence maps from the image matching stage to guide the densification to concentrate on higher-confidence points and get robust \mathcal{X}_d . In the final stage, our proposed *self-matching mechanism* further filters inconsistent patches, and the results are fed back into the densification stage for refinement. To further improve multi-view consistency, we train RGB-X 3DGS using COLMAP-calibrated RGB views to consolidate both modalities into a unified 3D RGB-X radiance field, which improves multi-view consistency and further enables cross-sensor view synthesis.

that conforms to known conditions \mathcal{X}_m and fills in unknown areas from \mathcal{I} and neighboring points.

Confidence-Aware Fusion. Naively densifying \mathcal{X}_m would lead to highly irregular structures due to uncertainty in image matching. To overcome the issue, we design Confidence-Aware Densification and Fusion (CADF) module that integrates the matching and densification stages by using the image-matching confidence c to improve the RGB-X densification.

First, we integrate c into DySPN refinement. The original DySPN formulates the recurrent iteration as follows: at timestep t , the refined result L^{t+1} combines current update L^t , weighted by affinity score w , and known points X_m , weighted by backbone-predicted certainty map C_s

$$L^{t+1} = (1 - C_s) \sum_r \sum_{(a,b)} w_{r,a,b} * L_{a,b}^t + C_s \mathcal{X}_m, \quad (3)$$

, where r denotes filters and (a, b) denotes the coordinates.

We propose to interleave the recurrent steps with the confidence map C_m from image matching that aggregates point confidence c into a map. C_m weighs down the contribution for probably incorrect original keypoints and concentrates the iterative refinement at the higher-confidence points.

$$L^{t+1} = (1 - C_s C_m) \sum_r \sum_{(a,b)} w_{r,a,b} * L_{a,b}^t + C_s C_m \mathcal{X}_m. \quad (4)$$

Next, we find that a higher δ keeps more robust points but leads to a sparser map that purely relies on RGB as cues for densification. A lower δ accepts more but noisy points as known conditions, which leads to irregular structures (See Supplementary for visuals). We perform K -level thresholding and fusion. Suppose we have K thresholds δ_k for

confidence c , thresholded keypoints $\mathcal{X}_{m,k}$, and their densified X-images $\hat{\mathcal{X}}_{d,k}, \forall k \in [1, K]$, we propose a fusion block F at the end of densification to fuse them. F is first pretrained on single-image enhancement to suppress noise, deblur, and sharpen edges. $\hat{\mathcal{X}}_{d,k}$ are input to F , and we mean pool over k to output \mathcal{X}_d , as the result for the CADF stage. We train F with self-supervised losses, including cosine similarity loss (Eq. 5) using SigLIP2 image encoder [78] along with RGB-X self-matching loss (Eq. 7)—both using RGB images to guide the enhancement and fusion for X-images.

$$\mathcal{L}_{\cos}(\mathcal{I}, \mathcal{X}_d) = 1 - \frac{f_{\text{SigLIP}}(\mathcal{I})^\top f_{\text{SigLIP}}(\mathcal{X}_d)}{\|f_{\text{SigLIP}}(\mathcal{I})\|_2 \|f_{\text{SigLIP}}(\mathcal{X}_d)\|_2}, \quad (5)$$

where both RGB and X are capturing the same scene that could be matched with the same descriptions, and thus the cosine similarity loss helps maximize feature map similarity.

3.3. Self-Matching Filtering and 3D Consolidation

Self-Matching. We propose a self-matching mechanism used both in fusion and the following filtering stage. Different from image matching—given two images, find a matching set that maps coordinates from one to another—now we have roughly aligned RGB-X pairs with the prior that coordinates in one image should map to the same locations in another. We can use the image matcher as a judge to evaluate whether the densified X-image is valid for matching to the same coordinates.

For training F , we look into the patch features from the transformer-based matcher and compute patch-level similarity matrix A , which is computed by scaled dot product of the RGB-X features.

$$A = \frac{F_{\mathcal{I}} F_{\mathcal{X}}^\top}{\tau}, \quad (6)$$

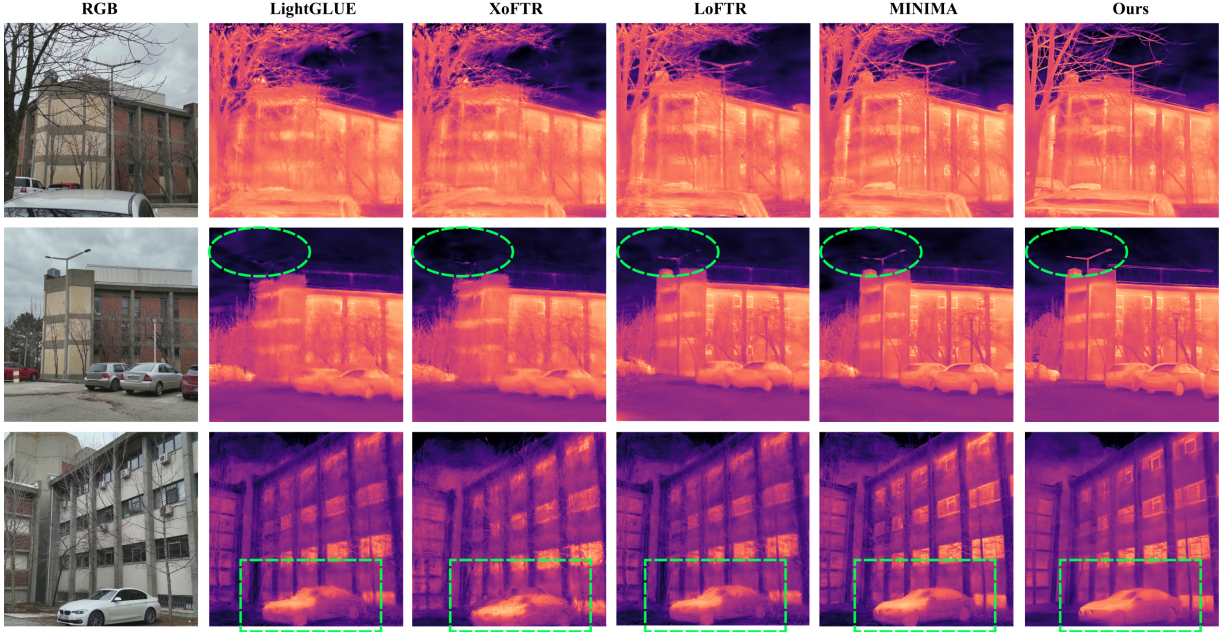


Figure 4. **Visual Results on METU-VisTIR-Cloudy.** Our results attain much clearer, sharper, and smoother surface for rendering.

where τ is a scale factor, and $F_{\mathcal{I}}$ and $F_{\mathcal{X}}$ are features for RGB and X in the coarse matching layer of the matcher [79].

The ideal similarity matrix should be diagonal. We compute the loss that maximizes the diagonal sum and minimizes the off-diagonal parts by

$$\mathcal{L}_{\text{sim}}(A) = -\frac{\text{Tr}(A)}{\|A\|_F} + \lambda \frac{\|A \odot (\hat{\mathbf{1}} - I)\|_1}{\|A\|_F}, \quad (7)$$

where $\|\cdot\|_F$ is the Frobenius norm, $\text{Tr}(\cdot)$ is trace for a matrix, I is the identity matrix, λ is a weight, and $\hat{\mathbf{1}}$ is the one-matrix. **Filtering.** We further use A to reject wrongly densified patches in \mathcal{X}_d . Looking into the diagonal of A , we compute a measure of concentration $q = \frac{Q_{50}(A)}{Q_{99}(A)}$, with $Q(\cdot)$ as the quantile function. A higher q indicates stronger self-matching results and thus fewer patches need to be rejected, while a lower q means the opposite. We take $(1-q)$ -quantile of A 's diagonal as the threshold and filter out patches of smaller scores.

Fine-Stage Densification. We then perform the fine-stage densification based on the filtered X-images. We follow the previous stage to perform densification without K -levels, and in Eq. 4 we take the normalized similarity score from A as C_m .

RGB-X 3DGS. To further make per-frame densification 3D-consistent, we consolidate the densified X-images by 3DGS [28, 38, 96]. We train RGB-X 3DGS, where we further add X-channels for each Gaussian. Unlike [36, 63], where they render multi-modality (e.g., color and language embedding) from separate channels and disentangle the GS parameters, here we just keep one set of parameters. Because

Table 1. **Results on METU-VisTIR-Cloudy.** Results are the mean of all six sequences. We compare with warping by different image matchers, all trained and rendered by 3DGS.

Method	Icos \uparrow	p30 \uparrow	p50 \uparrow	p70 \uparrow	p90 \uparrow	ITM \uparrow	ITcos \uparrow
XoFTR [79]	0.62	25.13	27.49	29.31	31.48	0.69	0.39
LightGlue [51]	0.61	25.89	28.28	30.14	32.35	0.91	0.40
LoFTR [74]	0.66	29.38	32.07	33.95	36.04	0.89	0.45
MINIMA _{lg} [66]	0.67	29.93	32.78	34.72	36.99	0.88	0.44
Ours	0.69	31.18	34.39	36.43	38.72	0.92	0.45

we find raw sensor imaging is often noisy or low-resolution, which cannot match the higher quality of RGB, and the latter can better position each 3D Gaussian precisely.

4. Experiments

X-Modalities and Datasets.

1. **RGB-Thermal.** The popular METU-VisTIR-Cloudy Dataset [79], which includes six sequences captured by *raw and unpaired* RGB and thermal sensors, is adopted for testing. We also use four scenes from RGBT-Scenes [54] containing paired RGB-thermal data for evaluation. We apply random rotation, shift, perspective warping, and radial distortion to create unpaired RGB-thermal data. To train D for this modality, we use synthetic RGB-thermal pairs created by MINIMA [66], which uses the MegaDepth Dataset [48] to create a large volume of paired data.

2. **RGB-NIR.** We adopt five sequences from RGB-NIR-Stereo [39], including one shorter and four extracted from two much longer sequences. We follow the same style as RGBT-Scenes to create unpaired data. To train D, we adopt

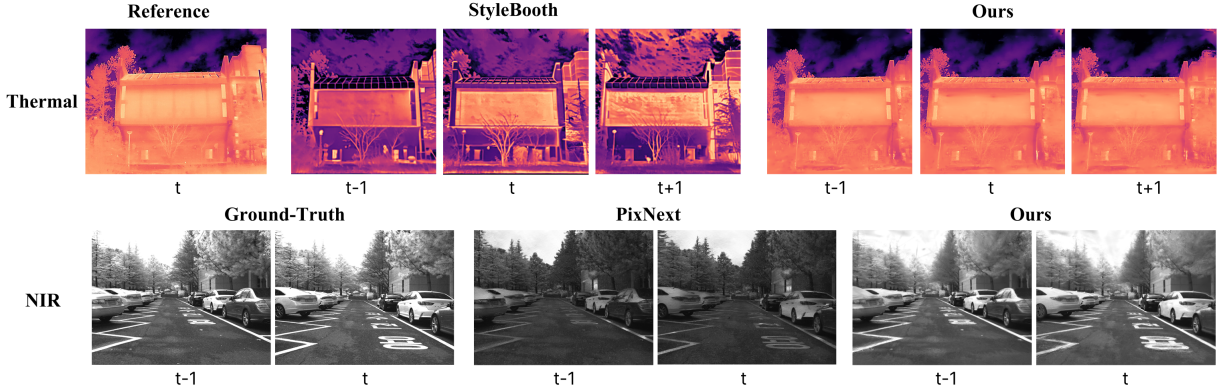


Figure 5. **Comparison on Temporal Consistency for Image Generation.** StyleBooth [25] generation for thermal images cannot guarantee temporal consistency due to inherent ambiguity, while ours densification creates more consistent multi-views. NIR is closer to the visual spectrum and thus easier to ensure consistency, but the specialized method PixNext [35] still cannot ensure the correct intensity. Compared with our strategy, image translation from the original domain still suffers from inaccurate transformations, whereas our match-densify-consolidate approach uses information from the target domain as anchors for densification and achieves better results.

Table 2. **Comparison on Temporal Consistency.** Compared with pure image generation, our match-densify-consolidate strategy obtains better multiview consistency from **lower** MET3R score.

MET3R↓	Sc1	Sc2	Sc3	Sc4	Sc5	Sc6	Mean
StyleBooth [25]	0.202	0.331	0.357	0.285	0.289	0.319	0.297
Ours	0.141	0.123	0.143	0.258	0.158	0.202	0.171

Deep-NIR [68] with synthetic paired RGB-NIR data.

3. RGB-SAR. We adopt three sub-Gigapixel satellite RGB-SAR pairs from DDHR-HK [65] and cut them into 512x512 patches for evaluation. We do not perform RGB-X 3DGS only on this modality since satellite images inherently cannot capture multi-view 3D. Several RGB-SAR datasets [10, 46, 91, 103] are used to train D.

Implementation Details. We adopt the transformer-based XoFTR [79] as the image matcher, which is trained on RGB-thermal but also presents strong ability for across different spectrum [66]. We choose $N = 7$ (-3 to +3 frame¹), $K = 3$ levels, $\delta = 0.15, 0.3, 0.5$, $\lambda = 0.1$, $\tau = 0.1$, and $c = 0.3$ for those area-sampled points. Fusion module F is an image-enhancement network [86] and pretrained on DIV2K [3] for image denoising, deblurring, and super-resolution. See Supplementary for details of training D and F.

Metrics. For datasets with only unpaired sequences without groundtruth, like METU-VisTIR-Cloudy, we calculate (1) image cosine similarity (Icos) for RGB-X image features from SigLIP-2 image encoder [78], (2) 30/50/70/90-percentile (p30-p90) on the diagonal of the similarity matrix of XoFTR for RGB-thermal, (3) image captioning and matching score— We use popular MLLM BLIP-2 [44] to first caption the RGB image and append ”, in a thermal im-

¹The work reasonably assumes rough alignment. A standard RGB-X data capture can trigger RGB-X shutters around the same time with similar scene coverage, but hard to be exact or aligned, as this is affected by on-the-fly system loading, physical displacement of sensors, or different intrinsics.

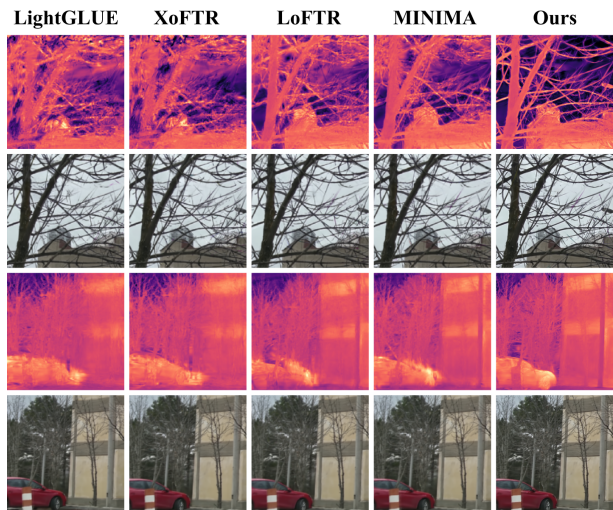


Figure 6. With the aid of sharper and clearer thermal images, the RGB view synthesis quality is also slightly enhanced.

age.” to the text. The caption and thermal images are used to calculate image-text matching score (ITM) and image-text cosine similarity (ITcos). Specifically, the match/mismatch score comes from a classification head that predicts two logits z_{match} and z_{mismatch} from its linear alignment. Then $\text{prob}_{\text{mismatch}} = \frac{e^{z_{\text{mismatch}}}}{e^{z_{\text{match}}} + e^{z_{\text{mismatch}}}}$.

For datasets with groundtruth, we calculate standard PSNR, SSIM, LPIPS as the fidelity scores, or RMSE/ MAE if the maps carry physical units such as °C. To evaluate temporal consistency, we use MET3R [4], which *lower scores* indicate *better multi-view consistency*.

Baselines. We include homography warping from different image matchers, including XoFTR [79], LightGLUE [51] LoFTR [74], and MINIMA_{tg} [66] as the featured matcher, followed by 3DGS training using their warped views. We also include cross-modal image generation, where models

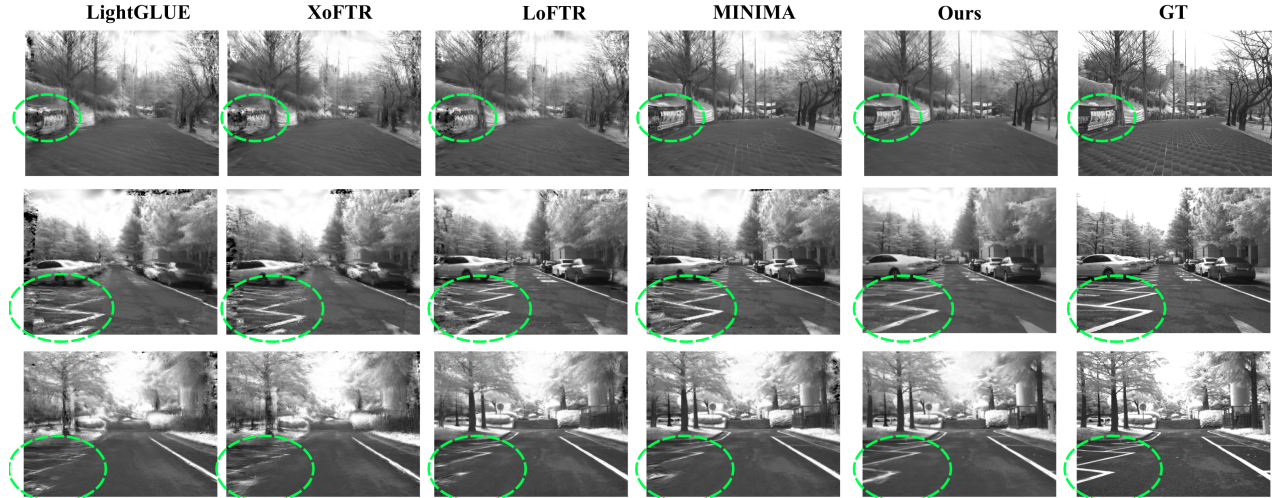


Figure 7. **Visual Results on RGB-NIR-Stereo.** Our view synthesis showcases better structures closer to the groundtruth (GT).

are trained with specific modalities, such as StyleBooth [25] used in [66] for RGB-thermal and [35] for RGB-NIR.

The work compares against the above methods without 3D priors for X, which aligns with our scope. We also consider 3D reprojection with estimated metric depth (from DepthAnythingV2 [94]), estimated camera pose (from essential matrix using matched keypoints), and groundtruth intrinsics for X. However, the pipeline cannot establish a reasonable baseline because metric depth and cross-modal camera pose estimation are far from robust in the wild [24, 88–90].

4.1. RGB-Thermal

METU-VisTIR-Cloudy. The dataset contains unpaired RGB and thermal sequences without groundtruth, and we adopt several metrics calculated against color images instead. See **Metrics**. From Tab. 1, our method consistently performs the best across all metrics, showing superior view-synthesis quality and faithful alignment with associated images. Especially for p30-p90, the higher similarity scores validate that our X-images make it easier for a pretrained image matcher to build correspondences. Fig. 4 shows a visual comparison, where our results show the most clear object structures of the thermal images. Further, we find that we also attain sharper RGB view synthesis (Fig. 6) than others due to better thermal images used in 3D consolidation.

We then compare with image generation from RGB views. We follow MINIMA [66], which uses StyleBooth [25] to craft paired RGB-thermal. Inherent ambiguity between appearance and true temperature makes it hard to estimate the exact temperature only from the appearance. This makes it unstable to generate consistent thermal images, while ours acquires true values by image matching and anchors those points in densification to synthesize views conforming to the true values. Tab. 2 shows that StyleBooth presents worse multiview consistency, where higher MET3R [4] indicates

Table 3. **Comparison on RGBT-Scenes.** We show results for train and novel view synthesis. Each scene reports RMSE \downarrow and MAE \downarrow in $^{\circ}\text{C}$. Novel views from the official split contain simpler views with lower errors than train views.

Train view	Building		Landscape		Parterre		RoadBlock		Mean	
	RMSE	MAE								
XoFTR [79]	2.50	1.81	1.08	0.79	2.25	1.57	1.21	0.93	1.76	1.28
LightGLUE [51]	2.48	1.79	1.10	0.81	2.28	1.57	1.26	0.97	1.78	1.29
LoFTR [74]	2.44	1.75	1.06	0.77	2.20	1.52	1.36	0.99	1.77	1.26
MINIMA [66]	2.51	1.83	1.08	0.80	2.35	1.66	1.36	1.04	1.83	1.33
Ours	2.43	1.72	1.02	0.71	2.18	1.49	1.18	0.91	1.70	1.21
Novel View	Building		Landscape		Parterre		RoadBlock		Mean	
	RMSE	MAE								
XoFTR [79]	2.70	1.92	1.02	0.70	1.34	0.84	0.47	0.40	1.38	0.97
LightGLUE [51]	2.78	2.00	1.01	0.73	1.21	0.71	0.85	0.68	1.46	1.03
LoFTR [74]	2.89	2.11	1.02	0.71	1.47	1.01	0.69	0.49	1.52	1.08
MINIMA [66]	2.55	1.78	0.98	0.65	0.91	0.58	0.33	0.26	1.19	0.82
Ours	2.33	1.70	0.97	0.66	0.81	0.55	0.35	0.27	1.12	0.80

worse consistency. Fig. 5 shows the differences in the upper. **RGBT-Scenes.** We follow the official split and report train and novel view synthesis results. Since the dataset contains paired RGB-thermal views with real temperatures, we compute RMSE and MAE in $^{\circ}\text{C}$ against groundtruth. Tab. 3 displays the results, where our method shows lower errors in nearly all sequences.

4.2. RGB-NIR

RGB-NIR-Stereo NIR captures the near-infrared spectrum, which is close to the visible range, and hence we compute regular image quality metrics, including PSNR, SSIM, and LPIPS, against groundtruth. Tab. 4 shows the comparison, where our method consistently achieves better scores across all the metrics, validating our pipeline. We show a visual comparison in Fig. 7, where our method produces better scene structure. In Fig. 5, the lower panel, we show a vi-

Table 4. **Results on RGB-NIR-Stereo.** Image quality metrics are shown. All methods are run with 3DGS.

Method	PSNR \uparrow	SSIM \uparrow	LPIPS \downarrow
PixNext [35]	11.283	0.441	0.452
XoFTR [79]	14.846	0.321	0.486
LightGlue [51]	16.253	0.377	0.455
LoFTR [74]	20.179	0.551	0.356
MINIMA [66]	20.392	0.568	0.360
Ours	21.152	0.581	0.344

Table 5. **Ablation Study.** We ablate each component in turn from the pipeline and report the average scores on RGB-NIR-Stereo.

Method	PSNR \uparrow	SSIM \uparrow	LPIPS \downarrow
Ours (final)	21.152	0.581	0.344
-3DGS	21.042	0.597	0.378
-Self-matching & filtering	20.235	0.522	0.386
-DySPN confidence	19.621	0.508	0.396
-Multi-level thresholds	19.215	0.495	0.420
-Area sampling	16.454	0.408	0.467

sual comparison to a RGB \rightarrow NIR image generation method, PixNext [35]. The method shows better generation consistency due to affinity to the visual spectrum, which makes image translation easier. But it still fails to produce the correct intensity compared to the groundtruth. This is also reflected in Tab. 4 with lower image quality scores.

Ablation Studies. We show ablation studies in Tab. 5, where we gradually remove each component and show the results, including 3DGS, self-matching and filtering, DySPN confidence, multi-level thresholds, and area sampling. From the table, each proposed component contributes to the final results. By integrating the image matching confidence into densification, the PSNR increases by 1dB. The self-matching and filtering help filter out poorly generated patches and condition on more robust points for re-densification, which accounts for 0.8dB improvement. 3DGS improves the performance and gets better view synthesis.

Pre-GS Comparison. We compare results without the final Gaussian Splatting, where we further discard the requirements for RGB camera poses and intrinsics from COLMAP. Tab. 6 shows the comparison, where all the methods in comparison are run without 3DGS. Our method still performs best. Notably, even without the GS-stage, we attain a mean PSNR of 21.042 (Tab. 5, also averaged from 5 sequences in Tab. 6), which is still better than all the methods run with 3DGS in Tab. 4. The results show that our sampling and CADF strategy is successful.

4.3. RGB-SAR

We conduct experiments on SAR view synthesis. We segment three DDHR-HK SAR and satellite images into overlapping 512x512 patches, and perform matching and den-

Table 6. **Comparison without 3DGS for all methods.** PSNR \uparrow on each sequence is shown on RGB-NIR-Stereo.

Method	09-28-16-48-17/1	09-28-16-48-17/2	09-28-17-06-04/1	09-28-17-06-04/2	10-26-15-53-03
PixNext [35]	11.19	11.99	12.81	12.22	8.65
XoFTR [79]	14.08	14.01	14.72	16.57	16.02
LightGlue [51]	14.03	14.10	14.61	16.67	16.07
LoFTR [74]	19.58	17.15	18.54	19.19	16.02
MINIMA [66]	21.16	18.80	19.67	21.76	19.70
Ours	21.47	20.27	20.24	22.67	20.56

Table 7. **Comparison DDHR-HK SAR.** We show image quality metrics against groundtruth.

Method	PSNR \uparrow	SSIM \uparrow	LPIPS \downarrow
XoFTR [79]	13.552	0.168	0.575
LoFTR [74]	13.462	0.164	0.615
LightGlue [51]	13.084	0.161	0.650
MINIMA [66]	14.849	0.229	0.377
Ours	17.102	0.302	0.339

sification on the patches. We do not perform 3DGS for all the methods in comparison and show image quality metrics against groundtruth. From Tab. 7, ours also scores the best in all metrics, demonstrating our superiority in this challenging task, where SAR signals are challenging for cross-modal matching. See Supplementary for more results, visualization including SAR’s, and other experiments, including feed-forward 3D reconstruction models and discussion on depth-projection.

5. Conclusion

We present the first study of cross-sensor view synthesis across different types of modalities—studying a practical, fundamental, yet widely overlooked problem in cross-modal learning on data alignment. We propose a novel and scalable framework in a match-densify-consolidate fashion to fulfill the goal, including integrating image matching and cross-modal densification together, using a carefully designed confidence guidance mechanism, a self-matching approach to further enhance quality, and consolidating cross-modalities in a unified 3D field. Extensive experiments on diverse sensor datasets validate our strategy. We expect the work to relieve the burden of sensor calibration and advance the popularity of cross-sensor learning in computer vision.

Limitations. First, the work focuses on static scenes and does not address dynamic objects, which is an issue in 3D consolidation and is still open for 3DGS research. Further, sensors such as thermal cameras are usually noisy and low-resolution [5]. Poor data quality can affect results and require in-domain denoising or enhancement on the signal level. Still, we rely on image matching and cannot solve extremely homogeneous cases without effective descriptors, a general bottleneck for matching-based solutions.

References

- [1] Rachael Abbott, Neil M Robertson, Jesus Martinez del Rincon, and Barry Connor. Unsupervised object detection via Iwir/rgb translation. In *Proceedings of the IEEE/CVF Conference on Computer Vision and Pattern Recognition Workshops*, pages 90–91, 2020. 2
- [2] NG Aditya, PB Dhruval, et al. Thermal voyager: A comparative study of rgb and thermal cameras for night-time autonomous navigation. In *2024 IEEE International Conference on Robotics and Automation (ICRA)*, pages 14116–14122. IEEE, 2024. 2
- [3] Eirikur Agustsson and Radu Timofte. Ntire 2017 challenge on single image super-resolution: Dataset and study. In *The IEEE Conference on Computer Vision and Pattern Recognition (CVPR) Workshops, 2017*. 6
- [4] Mohammad Asim, Christopher Wewer, Thomas Wimmer, Bernt Schiele, and Jan Eric Lenssen. Met3r: Measuring multi-view consistency in generated images. In *Proceedings of the Computer Vision and Pattern Recognition Conference*, pages 6034–6044, 2025. 6, 7
- [5] Arnaud Barral, Pablo Arias, and Axel Davy. Fixed pattern noise removal for multi-view single-sensor infrared camera. In *Proceedings of the IEEE/CVF Winter Conference on Applications of Computer Vision*, pages 1669–1678, 2024. 8
- [6] Amanda Berg, Jorgen Ahlberg, and Michael Felsberg. Generating visible spectrum images from thermal infrared. In *Proceedings of the IEEE Conference on Computer Vision and Pattern Recognition Workshops*, pages 1143–1152, 2018. 2
- [7] Mario Bijelic, Tobias Gruber, Fahim Mannan, Florian Kraus, Werner Ritter, Klaus Dietmayer, and Felix Heide. Seeing through fog without seeing fog: Deep multimodal sensor fusion in unseen adverse weather. In *Proceedings of the IEEE/CVF Conference on Computer Vision and Pattern Recognition*, pages 11682–11692, 2020. 2
- [8] Matthew Brown, Richard Szeliski, and Simon Winder. Multi-image matching using multi-scale oriented patches. In *2005 IEEE Computer Society Conference on Computer Vision and Pattern Recognition (CVPR'05)*, pages 510–517. IEEE, 2005. 3
- [9] Nicolas Bustos, Mehrsa Mashhadi, Susana K Lai-Yuen, Sudeep Sarkar, and Tapas K Das. A systematic literature review on object detection using near infrared and thermal images. *Neurocomputing*, 560:126804, 2023. 1
- [10] Ahmed Alejandro Cardona-Mesa, Rubén Darío Vásquez-Salazar, Luis Gómez, Carlos M Travieso-González, Andrés F Garavito-González, Esteban Vásquez-Cano, and Jean Pierre Díaz-Paz. Dataset of sentinel-1 sar and sentinel-2 rgb-ndvi imagery. *Data in Brief*, 57:111160, 2024. 6
- [11] Hongkai Chen, Zixin Luo, Lei Zhou, Yurun Tian, Mingmin Zhen, Tian Fang, David Mckinnon, Yanghai Tsin, and Long Quan. Aspanformer: Detector-free image matching with adaptive span transformer. In *European conference on computer vision*, pages 20–36. Springer, 2022. 3
- [12] Yukyung Choi, Namil Kim, Soonmin Hwang, Kibaek Park, Jae Shin Yoon, Kyoungwan An, and In So Kweon. Kaist multi-spectral day/night data set for autonomous and assisted driving. *IEEE Transactions on Intelligent Transportation Systems*, 19(3):934–948, 2018. 1
- [13] Sri Aditya Deevi, Connor Lee, Lu Gan, Sushruth Nagesh, Gaurav Pandey, and Soon-Jo Chung. Rgb-x object detection via scene-specific fusion modules. In *Proceedings of the IEEE/CVF Winter Conference on Applications of Computer Vision*, pages 7366–7375, 2024. 2
- [14] Fuqin Deng, Hua Feng, Mingjian Liang, Hongmin Wang, Yong Yang, Yuan Gao, Junfeng Chen, Junjie Hu, Xiyue Guo, and Tin Lun Lam. Feanet: Feature-enhanced attention network for rgb-thermal real-time semantic segmentation. In *2021 IEEE/RSJ international conference on intelligent robots and systems (IROS)*, pages 4467–4473. IEEE, 2021. 2
- [15] Yuxin Deng and Jiayi Ma. Redfeat: Recoupling detection and description for multimodal feature learning. *IEEE Transactions on Image Processing*, 32:591–602, 2022. 3
- [16] Mihai Dusmanu, Ignacio Rocco, Tomas Pajdla, Marc Pollefeys, Josef Sivic, Akihiko Torii, and Torsten Sattler. D2-net: A trainable cnn for joint description and detection of local features. In *Proceedings of the IEEE/CVF conference on computer vision and pattern recognition*, pages 8092–8101, 2019. 3
- [17] Johan Edstedt, Ioannis Athanasiadis, Mårten Wadenbäck, and Michael Felsberg. Dkm: Dense kernelized feature matching for geometry estimation. In *Proceedings of the IEEE/CVF Conference on Computer Vision and Pattern Recognition*, pages 17765–17775, 2023. 3
- [18] Johan Edstedt, Qiyu Sun, Georg Bökman, Mårten Wadenbäck, and Michael Felsberg. Roma: Robust dense feature matching. In *Proceedings of the IEEE/CVF Conference on Computer Vision and Pattern Recognition (CVPR)*, pages 19790–19800, 2024. 3
- [19] Ruoyu Fan, Wang Zhao, Matthieu Lin, Qi Wang, Yong-Jin Liu, and Wenping Wang. Generalizable thermal-based depth estimation via pre-trained visual foundation model. In *2024 IEEE International Conference on Robotics and Automation (ICRA)*, pages 14614–14621. IEEE, 2024. 1
- [20] Zhen Feng, Yanning Guo, and Yuxiang Sun. Cekd: Cross-modal edge-privileged knowledge distillation for semantic scene understanding using only thermal images. *IEEE Robotics and Automation Letters*, 8(4):2205–2212, 2023. 2
- [21] Martin A Fischler and Robert C Bolles. Random sample consensus: a paradigm for model fitting with applications to image analysis and automated cartography. *Communications of the ACM*, 24(6):381–395, 1981. 3
- [22] Gianni Franchi, Marwane Hariat, Xuanlong Yu, Nacim Belkhir, Antoine Manzanera, and David Filliat. Infraparis: A multi-modal and multi-task autonomous driving dataset. In *Proceedings of the IEEE/CVF Winter Conference on Applications of Computer Vision*, pages 2973–2983, 2024. 1
- [23] Oriol Frigo, Lucien Martin-Gaffe, and Catherine Wacogne. Doodlenet: Double deeplab enhanced feature fusion for thermal-color semantic segmentation. In *Proceedings of the IEEE/CVF Conference on Computer Vision and Pattern Recognition*, pages 3021–3029, 2022. 2
- [24] Yuliang Guo, Sparsh Garg, S Mahdi H Miangoleh, Xinyu Huang, and Liu Ren. Depth any camera: Zero-shot metric

- depth estimation from any camera. In *Proceedings of the Computer Vision and Pattern Recognition Conference*, pages 26996–27006, 2025. 7
- [25] Zhen Han, Chaojie Mao, Zeyinzi Jiang, Yulin Pan, and Jingfeng Zhang. Stylebooth: Image style editing with multi-modal instruction. In *Proceedings of the IEEE/CVF International Conference on Computer Vision (ICCV) Workshops*, pages 1947–1957, 2025. 6, 7
- [26] Lingyi Hong, Shilin Yan, Renrui Zhang, Wanyun Li, Xinyu Zhou, Pinxue Guo, Kaixun Jiang, Yiting Chen, Jinglun Li, Zhaoyu Chen, et al. Onetracker: Unifying visual object tracking with foundation models and efficient tuning. In *Proceedings of the IEEE/CVF conference on computer vision and pattern recognition*, pages 19079–19091, 2024. 2
- [27] Xiaojun Hou, Jiazheng Xing, Yijie Qian, Yaowei Guo, Shuo Xin, Junhao Chen, Kai Tang, Mengmeng Wang, Zhengkai Jiang, Liang Liu, et al. Sdstrack: Self-distillation symmetric adapter learning for multi-modal visual object tracking. In *Proceedings of the IEEE/CVF Conference on Computer Vision and Pattern Recognition*, pages 26551–26561, 2024. 2
- [28] Zixun Huang, Cho-Ying Wu, Yuliang Guo, Xinyu Huang, and Liu Ren. 3dgeer: 3d gaussian rendering made exact and efficient for generic cameras. In *The Fourteenth International Conference on Learning Representations*, 2026. 5
- [29] Tianrui Hui, Zizheng Xun, Fengguang Peng, Junshi Huang, Xiaoming Wei, Xiaolin Wei, Jiao Dai, Jizhong Han, and Si Liu. Bridging search region interaction with template for rgb-t tracking. In *Proceedings of the IEEE/CVF Conference on Computer Vision and Pattern Recognition*, pages 13630–13639, 2023. 2
- [30] Mohd Shawal Jadin and Kamarul Hawari Ghazali. Gas leakage detection using thermal imaging technique. In *2014 UKSim-AMSS 16th International Conference on Computer Modelling and Simulation*, pages 302–306. IEEE, 2014. 1
- [31] Wei Ji, Jingjing Li, Cheng Bian, Zongwei Zhou, Jiaying Zhao, Alan L Yuille, and Li Cheng. Multispectral video semantic segmentation: A benchmark dataset and baseline. In *Proceedings of the IEEE/CVF Conference on Computer Vision and Pattern Recognition*, pages 1094–1104, 2023. 2
- [32] Hanwen Jiang, Arjun Karapur, Bingyi Cao, Qixing Huang, and André Araujo. Omniglue: Generalizable feature matching with foundation model guidance. In *Proceedings of the IEEE/CVF Conference on Computer Vision and Pattern Recognition (CVPR)*, pages 19865–19875, 2024. 3
- [33] Jiajun Jiang, Xingxin Chen, Weichen Dai, Zelin Gao, and Yu Zhang. Thermal-inertial slam for the environments with challenging illumination. *IEEE Robotics and Automation Letters*, 7(4):8767–8774, 2022. 2
- [34] Shuangping Jin, Bingbing Yu, Minhao Jing, Yi Zhou, Jiajun Liang, and Renhe Ji. Darkvisionnet: Low-light imaging via rgb-nir fusion with deep inconsistency prior. In *Proceedings of the AAAI Conference on Artificial Intelligence*, pages 1104–1112, 2022. 2
- [35] Youngwan Jin, Incheol Park, Hanbin Song, Hyeongjin Ju, Yagiz Nalcakan, and Shiho Kim. Pix2next: Leveraging vision foundation models for rgb to nir image translation. *Technologies*, 2025. 6, 7, 8
- [36] Saimouli Katragadda, Cho-Ying Wu, Yuliang Guo, Xinyu Huang, Guoquan Huang, and Liu Ren. Online language splatting. In *Proceedings of the IEEE/CVF International Conference on Computer Vision (ICCV)*, 2025. 5
- [37] Nikhil Keetha, Norman Müller, Johannes Schönberger, Lorenzo Porzi, Yuchen Zhang, Tobias Fischer, Arno Knapitsch, Duncan Zauss, Ethan Weber, Nelson Antunes, et al. Mapanything: Universal feed-forward metric 3d reconstruction. In *3DV*, 2026. 3
- [38] Bernhard Kerbl, Georgios Kopanas, Thomas Leimkühler, George Drettakis, et al. 3d gaussian splatting for real-time radiance field rendering. *ACM Trans. Graph.*, 42(4):139–1, 2023. 5
- [39] Jinnyeong Kim and Seung-Hwan Baek. Pixel-aligned rgb-nir stereo imaging and dataset for robot vision. In *Proceedings of the Computer Vision and Pattern Recognition Conference*, pages 11482–11492, 2025. 1, 5
- [40] Janghyun Kim, Ukcheol Shin, Seokyong Heo, and Jinsun Park. Exploiting cross-modal cost volume for multi-sensor depth estimation. In *Proceedings of the Asian Conference on Computer Vision*, pages 1420–1436, 2024. 2
- [41] Da Kong, Yu Zhang, and Weichen Dai. Direct near-infrared-depth visual slam with active lighting. *IEEE Robotics and Automation Letters*, 6(4):7057–7064, 2021. 2
- [42] Chenglong Li, Lei Liu, Andong Lu, Qing Ji, and Jin Tang. Challenge-aware rgbt tracking. In *European conference on computer vision*, pages 222–237. Springer, 2020. 2
- [43] Haotian Li, Henry K Chu, and Yuxiang Sun. Improving rgb-thermal semantic scene understanding with synthetic data augmentation for autonomous driving. *IEEE Robotics and Automation Letters*, 2025. 1
- [44] Junnan Li, Dongxu Li, Silvio Savarese, and Steven Hoi. Blip-2: Bootstrapping language-image pre-training with frozen image encoders and large language models. In *International conference on machine learning*, pages 19730–19742. PMLR, 2023. 6
- [45] Ting Li, Mao Ye, Tianwen Wu, Nianxin Li, Shuaifeng Li, Song Tang, and Luping Ji. Pseudo visible feature fine-grained fusion for thermal object detection. In *Proceedings of the Computer Vision and Pattern Recognition Conference*, pages 6710–6719, 2025. 2
- [46] Xue Li, Guo Zhang, Hao Cui, Shasha Hou, Shun Yao Wang, Xin Li, Yujia Chen, Zhijiang Li, and Li Zhang. Mcanet: A joint semantic segmentation framework of optical and sar images for land use classification. *International Journal of Applied Earth Observation and Geoinformation*, 106:102638, 2022. 6
- [47] You Li, Julien Moreau, and Javier Ibanez-Guzman. Emergent visual sensors for autonomous vehicles. *IEEE Transactions on Intelligent Transportation Systems*, 24(5):4716–4737, 2023. 1
- [48] Zhengqi Li and Noah Snavely. Megadepth: Learning single-view depth prediction from internet photos. In *Proceedings of the IEEE conference on computer vision and pattern recognition*, pages 2041–2050, 2018. 5

- [49] Mingjian Liang, Junjie Hu, Chenyu Bao, Hua Feng, Fuqin Deng, and Tin Lun Lam. Explicit attention-enhanced fusion for rgb-thermal perception tasks. *IEEE Robotics and Automation Letters*, 8(7):4060–4067, 2023. 2
- [50] Yuankai Lin, Tao Cheng, Qi Zhong, Wending Zhou, and Hua Yang. Dynamic spatial propagation network for depth completion. In *Proceedings of the AAAI conference on artificial intelligence*, pages 1638–1646, 2022. 3
- [51] Philipp Lindenberger, Paul-Edouard Sarlin, and Marc Pollefeys. Lightglue: Local feature matching at light speed. In *Proceedings of the IEEE/CVF international conference on computer vision*, pages 17627–17638, 2023. 3, 5, 6, 7, 8
- [52] Jinyuan Liu, Zhu Liu, Guanyao Wu, Long Ma, Risheng Liu, Wei Zhong, Zhongxuan Luo, and Xin Fan. Multi-interactive feature learning and a full-time multi-modality benchmark for image fusion and segmentation. In *Proceedings of the IEEE/CVF international conference on computer vision*, pages 8115–8124, 2023. 2
- [53] Jinyuan Liu, Guanyao Wu, Zhu Liu, Di Wang, Zhiying Jiang, Long Ma, Wei Zhong, and Xin Fan. Infrared and visible image fusion: From data compatibility to task adaption. *IEEE Transactions on Pattern Analysis and Machine Intelligence*, 2024. 2
- [54] Rongfeng Lu, Hangyu Chen, Zunjie Zhu, Yuhang Qin, Ming Lu, Chenggang Yan, et al. Thermalgaussian: Thermal 3d gaussian splatting. In *The Thirteenth International Conference on Learning Representations*, 2025. 2, 5
- [55] Rishabh Madan, Skyler Valdez, David Kim, Sujie Fang, Luoyan Zhong, Diego T Virtue, and Tapomayukh Bhat-tacharjee. Rabbit: A robot-assisted bed bathing system with multimodal perception and integrated compliance. In *Proceedings of the 2024 ACM/IEEE international conference on human-robot interaction*, pages 472–481, 2024. 2
- [56] Jonas Mirlach, Lei Wan, Andreas Wiedholz, Hannan Ejaz Keen, and Andreas Eich. R-livit: A lidar-visual-thermal dataset enabling vulnerable road user focused roadside perception. In *ICCV*, 2025. 1
- [57] Farzeen Munir, Shoaib Azam, and Moongu Jeon. Sstn: Self-supervised domain adaptation thermal object detection for autonomous driving. In *2021 IEEE/RSJ international conference on intelligent robots and systems (IROS)*, pages 206–213. IEEE, 2021. 1
- [58] Farzeen Munir, Shoaib Azam, Muhammad Aasim Rafique, Ahmad Muqem Sheri, Moongu Jeon, and Witold Pedrycz. Exploring thermal images for object detection in underexposure regions for autonomous driving. *Applied soft computing*, 121:108793, 2022. 1
- [59] Junjie Ni, Guofeng Zhang, Guanglin Li, Yijin Li, Xinyang Liu, Zhaoyang Huang, and Hujun Bao. Eto: Efficient transformer-based local feature matching by organizing multiple homography hypotheses. *Advances in Neural Information Processing Systems*, 37:60260–60274, 2024. 3
- [60] Yuki Ono, Eduard Trulls, Pascal Fua, and Kwang Moo Yi. Lf-net: Learning local features from images. *Advances in neural information processing systems*, 31, 2018. 3
- [61] Edoardo Palladin, Roland Dietze, Praveen Narayanan, Mario Bijelic, and Felix Heide. Samfusion: Sensor-adaptive multi-modal fusion for 3d object detection in adverse weather. In *European Conference on Computer Vision*, pages 484–503. Springer, 2024. 2
- [62] Jay N Paranjape, Celso de Melo, and Vishal M Patel. F-vita: Foundation model guided visible to thermal translation. *arXiv preprint arXiv:2504.02801*, 2025. 1
- [63] Qucheng Peng, Benjamin Planche, Zhongpai Gao, Meng Zheng, Anwesa Choudhuri, Terrence Chen, Chen Chen, and Ziyang Wu. 3d vision-language gaussian splatting. In *The Thirteenth International Conference on Learning Representations*, 2025. 5
- [64] Guilherme Potje, Felipe Cadar, André Araujo, Renato Martins, and Erickson R Nascimento. Xfeat: Accelerated features for lightweight image matching. In *Proceedings of the IEEE/CVF Conference on Computer Vision and Pattern Recognition*, pages 2682–2691, 2024. 3
- [65] Bo Ren, Shibin Ma, Biao Hou, Danfeng Hong, Jocelyn Chanussot, Jianlong Wang, and Licheng Jiao. A dual-stream high resolution network: Deep fusion of gf-2 and gf-3 data for land cover classification. *International Journal of Applied Earth Observation and Geoinformation*, 112:102896, 2022. 6
- [66] Jiangwei Ren, Xingyu Jiang, Zizhuo Li, Dingkang Liang, Xin Zhou, and Xiang Bai. Minima: Modality invariant image matching. In *Proceedings of the Computer Vision and Pattern Recognition Conference*, pages 23059–23068, 2025. 2, 3, 5, 6, 7, 8
- [67] Tianhe Ren, Shilong Liu, Ailing Zeng, Jing Lin, Kunchang Li, He Cao, Jiayu Chen, Xinyu Huang, Yukang Chen, Feng Yan, et al. Grounded sam: Assembling open-world models for diverse visual tasks. *arXiv preprint arXiv:2401.14159*, 2024. 3
- [68] Inkyu Sa, Jong Yoon Lim, Ho Seok Ahn, and Bruce MacDonald. deepnir: Datasets for generating synthetic nir images and improved fruit detection system using deep learning techniques. *Sensors*, 22(13):4721, 2022. 6
- [69] Paul-Edouard Sarlin, Daniel DeTone, Tomasz Malisiewicz, and Andrew Rabinovich. Superglue: Learning feature matching with graph neural networks. In *Proceedings of the IEEE/CVF conference on computer vision and pattern recognition*, pages 4938–4947, 2020. 3
- [70] Johannes L Schonberger and Jan-Michael Frahm. Structure-from-motion revisited. In *Proceedings of the IEEE conference on computer vision and pattern recognition*, pages 4104–4113, 2016. 1
- [71] Furqan Ahmed Shaik, Abhishek Reddy, Nikhil Reddy Billa, Kunal Chaudhary, Sunny Manchanda, and Girish Varma. Idd-aw: A benchmark for safe and robust segmentation of drive scenes in unstructured traffic and adverse weather. In *Proceedings of the IEEE/CVF Winter Conference on Applications of Computer Vision*, pages 4614–4623, 2024. 2
- [72] Yan Shi, Jun-Xiong Cai, Yoli Shavit, Tai-Jiang Mu, Wensen Feng, and Kai Zhang. Clustergnn: Cluster-based coarse-to-fine graph neural network for efficient feature matching. In *Proceedings of the IEEE/CVF conference on computer vision and pattern recognition*, pages 12517–12526, 2022. 3
- [73] Ukcheol Shin, Jinsun Park, and In So Kweon. Deep depth estimation from thermal image. In *Proceedings of the*

- IEEE/CVF Conference on Computer Vision and Pattern Recognition*, pages 1043–1053, 2023. 2
- [74] Jiaming Sun, Zehong Shen, Yuang Wang, Hujun Bao, and Xiaowei Zhou. Loftr: Detector-free local feature matching with transformers. In *Proceedings of the IEEE/CVF conference on computer vision and pattern recognition*, pages 8922–8931, 2021. 3, 5, 6, 7, 8
- [75] Yuxiang Sun, Weixun Zuo, and Ming Liu. Rtfnet: Rgb-thermal fusion network for semantic segmentation of urban scenes. *IEEE Robotics and Automation Letters*, 4(3):2576–2583, 2019. 2
- [76] Hao Tang, Zechao Li, Dong Zhang, Shengfeng He, and Jinhui Tang. Divide-and-conquer: Confluent triple-flow network for rgb-t salient object detection. *IEEE Transactions on Pattern Analysis and Machine Intelligence*, 2024. 2
- [77] Engin Tola, Vincent Lepetit, and Pascal Fua. A fast local descriptor for dense matching. In *2008 IEEE conference on computer vision and pattern recognition*, pages 1–8. IEEE, 2008. 3
- [78] Michael Tschannen, Alexey Gritsenko, Xiao Wang, Muhammad Ferjad Naeem, Ibrahim Alabdulmohsin, Nikhil Parthasarathy, Talfan Evans, Lucas Beyer, Ye Xia, Basil Mustafa, et al. Siglip 2: Multilingual vision-language encoders with improved semantic understanding, localization, and dense features. *arXiv preprint arXiv:2502.14786*, 2025. 4, 6
- [79] Önder Tuzcuoğlu, Aybora Köksal, Buğra Sofu, Sinan Kalkan, and A Aydin Alatan. Xoftr: Cross-modal feature matching transformer. In *Proceedings of the IEEE/CVF conference on computer vision and pattern recognition Workshops*, pages 4275–4286, 2024. 2, 3, 5, 6, 7, 8
- [80] Michał Tyszkiewicz, Pascal Fua, and Eduard Trulls. Disk: Learning local features with policy gradient. *Advances in neural information processing systems*, 33:14254–14265, 2020. 3
- [81] Zifu Wan, Pingping Zhang, Yuhao Wang, Silong Yong, Simon Stepputtis, Katia Sycara, and Yaqi Xie. Sigma: Siamese mamba network for multi-modal semantic segmentation. In *2025 IEEE/CVF Winter Conference on Applications of Computer Vision (WACV)*, pages 1734–1744. IEEE, 2025. 2
- [82] Bing Wang, Changhao Chen, Zhaopeng Cui, Jie Qin, Chris Xiaoxuan Lu, Zhengdi Yu, Peijun Zhao, Zhen Dong, Fan Zhu, Niki Trigoni, et al. P2-net: Joint description and detection of local features for pixel and point matching. In *Proceedings of the IEEE/CVF International Conference on Computer Vision*, pages 16004–16013, 2021. 3
- [83] Jianyuan Wang, Minghao Chen, Nikita Karaev, Andrea Vedaldi, Christian Rupprecht, and David Novotny. Vggt: Visual geometry grounded transformer. In *Proceedings of the Computer Vision and Pattern Recognition Conference*, pages 5294–5306, 2025. 3
- [84] Qing Wang, Jiaming Zhang, Kailun Yang, Kunyu Peng, and Rainer Stiefelhagen. Matchformer: Interleaving attention in transformers for feature matching. In *Proceedings of the Asian conference on computer vision*, pages 2746–2762, 2022. 3
- [85] Shuzhe Wang, Vincent Leroy, Yohann Cabon, Boris Chidlovskii, and Jerome Revaud. Dust3r: Geometric 3d vision made easy. In *Proceedings of the IEEE/CVF Conference on Computer Vision and Pattern Recognition*, pages 20697–20709, 2024. 3
- [86] Yan Wang. Edge-enhanced feature distillation network for efficient super-resolution. In *Proceedings of the IEEE/CVF Conference on Computer Vision and Pattern Recognition (CVPR) Workshops*, pages 777–785, 2022. 6
- [87] Cho-Ying Wu and Ulrich Neumann. Scene completeness-aware lidar depth completion for driving scenario. In *ICASSP 2021-2021 IEEE International Conference on Acoustics, Speech and Signal Processing (ICASSP)*, pages 2490–2494. IEEE, 2021. 2
- [88] Cho-Ying Wu, Jialiang Wang, Michael Hall, Ulrich Neumann, and Shuochen Su. Toward practical monocular indoor depth estimation. In *Proceedings of the IEEE/CVF Conference on Computer Vision and Pattern Recognition (CVPR)*, pages 3814–3824, 2022. 7
- [89] Cho-Ying Wu, Quankai Gao, Chin-Cheng Hsu, Te-Lin Wu, Jing-Wen Chen, and Ulrich Neumann. Inspacetype: Reconsider space type in indoor monocular depth estimation. In *The British Machine Vision Conference (BMVC)*, 2024.
- [90] Cho-Ying Wu, Yiqi Zhong, Junying Wang, and Ulrich Neumann. Boosting generalizability towards zero-shot cross-dataset single-image indoor depth by meta-initialization. In *2024 IEEE/RSJ International Conference on Intelligent Robots and Systems (IROS)*, pages 10051–10058. IEEE, 2024. 7
- [91] Yuming Xiang, Rongshu Tao, Feng Wang, Hongjian You, and Bing Han. Automatic registration of optical and sar images via improved phase congruency model. *IEEE Journal of Selected Topics in Applied Earth Observations and Remote Sensing*, 13:5847–5861, 2020. 6
- [92] JiuHong Xiao, Roshan Nayak, Ning Zhang, Daniel Tortei, and Giuseppe Loianno. Thermalgen: Style-disentangled flow-based generative models for rgb-to-thermal image translation. *arXiv preprint arXiv:2509.24878*, 2025. 2
- [93] Qin Xu, Yiming Mei, Jinpei Liu, and Chenglong Li. Multi-modal cross-layer bilinear pooling for rgb-t tracking. *IEEE Transactions on Multimedia*, 24:567–580, 2021. 2
- [94] Lihe Yang, Bingyi Kang, Zilong Huang, Zhen Zhao, Xiaogang Xu, Jiashi Feng, and Hengshuang Zhao. Depth anything v2. *Advances in Neural Information Processing Systems*, 37:21875–21911, 2024. 7
- [95] Meng Yang, Fan Fan, Zizhuo Li, Songchu Deng, Yong Ma, and Jiayi Ma. Distillmatch: Leveraging knowledge distillation from vision foundation model for multimodal image matching. *arXiv preprint arXiv:2509.16017*, 2025. 2
- [96] Zehao Yu, Anpei Chen, Binbin Huang, Torsten Sattler, and Andreas Geiger. Mip-splatting: Alias-free 3d gaussian splatting. In *Proceedings of the IEEE/CVF conference on computer vision and pattern recognition*, pages 19447–19456, 2024. 5
- [97] Jiaming Zhang, Huayao Liu, Kailun Yang, Xinxin Hu, Ruiping Liu, and Rainer Stiefelhagen. Cmx: Cross-modal fusion for rgb-x semantic segmentation with transformers. *IEEE Transactions on intelligent transportation systems*, 24(12):14679–14694, 2023. 2

- [98] Pengyu Zhang, Jie Zhao, Dong Wang, Huchuan Lu, and Xiang Ruan. Visible-thermal uav tracking: A large-scale benchmark and new baseline. In *Proceedings of the IEEE/CVF Conference on Computer Vision and Pattern Recognition*, pages 8886–8895, 2022. 2
- [99] Qiang Zhang, Shenlu Zhao, Yongjiang Luo, Dingwen Zhang, Nianchang Huang, and Jungong Han. Abmdrnet: Adaptive-weighted bi-directional modality difference reduction network for rgb-t semantic segmentation. In *Proceedings of the IEEE/CVF Conference on Computer Vision and Pattern Recognition*, pages 2633–2642, 2021. 2
- [100] Tianlu Zhang, Hongyuan Guo, Qiang Jiao, Qiang Zhang, and Jungong Han. Efficient rgb-t tracking via cross-modality distillation. In *Proceedings of the IEEE/CVF conference on computer vision and pattern recognition*, pages 5404–5413, 2023. 2
- [101] Zhen Zhang and Wee Sun Lee. Deep graphical feature learning for the feature matching problem. In *Proceedings of the IEEE/CVF International Conference on Computer Vision*, pages 5087–5096, 2019. 3
- [102] Jiayi Zhao, Fei Teng, Kai Luo, Guoqiang Zhao, Zhiyong Li, Xu Zheng, and Kailun Yang. Unveiling the potential of segment anything model 2 for rgb-thermal semantic segmentation with language guidance. *IEEE/RSJ international conference on intelligent robots and systems (IROS)*, 2025. 1
- [103] Xuyang Zhao, Lijun Zhao, Hongyi Li, Zheng Zhang, and Ping Tang. A multimodal visible-sar dataset for airport detection in remote sensing imagery. Science Data Bank, Dataset, Version 1.0, 2025. Available at <https://doi.org/10.57760/sciencedb.j00001.01276>. 6
- [104] Xu Zheng, Yuanhuiyi Lyu, and Lin Wang. Learning modality-agnostic representation for semantic segmentation from any modalities. In *European Conference on Computer Vision*, pages 146–165. Springer, 2024. 2
- [105] Wujie Zhou, Jinfu Liu, Jingsheng Lei, Lu Yu, and Jenq-Neng Hwang. Gmnet: Graded-feature multilabel-learning network for rgb-thermal urban scene semantic segmentation. *IEEE Transactions on Image Processing*, 30:7790–7802, 2021. 2
- [106] Yiming Zuo and Jia Deng. Ogni-dc: Robust depth completion with optimization-guided neural iterations. In *European Conference on Computer Vision*, pages 78–95. Springer, 2024. 3
- [107] Yiming Zuo, Willow Yang, Zeyu Ma, and Jia Deng. Omni-dc: Highly robust depth completion with multiresolution depth integration. In *Proceedings of the IEEE/CVF International Conference on Computer Vision*, pages 9287–9297, 2025. 3